Journal of Computational Mathematics
Vol.xx, No.x, 2023, 1–21.
http://www.global-sci.org/jcm
doi:10.4208/jcm.2212-m2021-0231

A COUPLED METHOD COMBINING CROUZEIX-RAVIART NONCONFORMING AND NODE CONFORMING FINITE ELEMENT SPACES FOR BOIT CONSOLIDATION MODEL*

Yuping Zeng
School of Mathematics, Jiaying University, Meizhou 514015, China
Email: zeng_yuping@163.com
Mingchao Cai
Department of Mathematics, Morgan State University, 1700 E Cold Spring Ln, Baltimore, MD 21251, USA
Email: cmchao2005@gmail.com
Liuqiang Zhong[1)]
School of Mathematical Science, South China Normal University, Guangzhou 520631, Guangdong, China
Email: zhong@scnu.edu.cn

Abstract

A mixed finite element method is presented for the Biot consolidation problem in poroelasticity. More precisely, the displacement is approximated by using the Crouzeix-Raviart nonconforming finite elements, while the fluid pressure is approximated by using the node conforming finite elements. The well-posedness of the fully discrete scheme is established, and a corresponding priori error estimate with optimal order in the energy norm is also derived. Numerical experiments are provided to validate the theoretical results.

Mathematics subject classification: 65N15, 65M60, 74F10.
Key words: Poroelasticity, Nonconforming finite element, Inf-sup condition, A priori error estimate.

1. Introduction

Poroelasticity describes the interaction between a fluid flow and a deformable elastic porous medium that is saturated in the fluid. Its theoretical basis was initially established by Biot [4]. Biot poroelastic theory can be found in a wide range of applications. For example, the mathematical models for land subsidence in geomechanics [11, 45], carbon sequestration [43, 44, 46], safe long-term disposal of wastes in environment engineering [43, 46], and brain edema [29], are all poroelastic models.

In the context of numerical treatments for poroelastic equations, finite element methods (FEMs) are the most commonly used approaches [40, 41]. It is well known that a direct continuous Galerkin approximation may cause Poisson locking or nonphysical pressure oscillations (we call these two phenomenons as poroelaticity locking) [21, 42–44, 46]. In the literature, there have been some developed numerical methods to avoid the poroelaticity locking. We review those which motivated our work: A two-field formulation of the Biot model with the elastic displacement and pressure being unknowns was approximated by using the MINI element with

* Received August 10, 2021 / Revised version received February 22, 2022 / Accepted December 20, 2022 / Published online May 31, 2023 /
1) Corresponding author

a stabilization term [48]. With the same formulation, discontinuous Galerkin (DG) methods, weak Galerkin methods and hybrid high order methods were developed in [5, 13, 14, 26, 52]. By introducing an additional fluid flux variable, a new three-field formulation was obtained, and a numerical method that couples DG methods and mixed FEMs was investigated in [45]. Later, this method was extended to nonconforming FEMs [27, 36, 54], virtual element methods [51], weak Galerkin methods [50], locally conservative DG methods [24, 30, 56]. Some numerical schemes based on four-field formulation can be found in [33, 35, 55]. Interested readers can also refer to [10, 11, 19, 31, 32] for other study of locking-free numerical methods for the Biot model. Moreover, for the corresponding fast solvers, some preconditioners which are robust with respect to the physical and discretization parameters have been developed in [1, 3, 12, 25, 37]. As mentioned above, the key issue in the numerical solution of the Biot problem is to address two numerical instabilities: Possion locking phenomenon and nonphysical pressure oscillations. In the two-field formulation these two instabilities have been initially discussed in the earlier works [40–42] from the regularity point of view. Therein they utilized inf-sup stabilized Stokes FEMs to discretize equations. However, recently it is shown in [2,48] that only inf-sup condition is not enough to overcome nonphysical pressure oscillations. They suggested adding a time-dependent stabilization term to address this issue. On the other hand, in the case of three-field formulation, the authors in [46] combine numerical tests with heuristic analysis to explain that the poroelasticity locking typically occurs when the storage coefficient is very close to zero and the small time step is used. In such a case, the poroelasticity model behaves as an incompressible model. For a remedy, they suggested using DG scheme or nonconforming FEM to approximate the displacement variable [45]. Though many works have been devoted to addressing these issues, most of them only numerically verify whether the constructed elements are locking-free or pressure-oscillations free, the corresponding mathematical justifications and interpretations behind these methods are relatively rare. More recently, an interesting result in [24] concluded that, in the three-field formulation, when the FE pairs for the displacements, Darcy velocity, and pore pressure satisfy suitable compatibilities, one can obtain a family of parameter-robust numerical schemes. In the same formulation, another breakthrough in the theoretical aspect can be found in a recent paper [55], in which the regularity of the Biot model is firstly obtained, the cause of pressure oscillations is reinvestigated from an algebraic viewpoint, and the Poisson locking is viewed from the classical FE approximation of linear elasticity. Moreover, based on the theoretical analysis, the author of [55] developed a new three-field mixed FEM that is free of locking and nonphysical pressure oscillations. The objective of the present work is to design a robust two-field FEM for the Biot model. We shall use the nonconforming Crouzeix-Raviart (CR) [15] finite element to approximate the elastic displacement, and adopt the standard linear continuous finite element for the pore pressure. It is shown that the error order estimate is robust with respect to the Lamé constant λ (more details can be found in Remark 5.3 in Section 5). In other words, we give a mathematical analysis that explains why nonconforming CR FEM displacement discretization can overcome Possion locking in poroelasticity. In addition, motivated by [48], a stabilization term is imposed in order to remove the nonphysical pressure oscillations arising from the continuous FE approximation. The finite element pair used in this article was initially proposed and analyzed for Stokes problems [38], in which a stabilization was suggested. Later, Lamichhane pointed out that the stabilization proposed in [38] is unnecessary [34]. It means that such a finite element pair satisfies the inf-sup condition for Stokes equations. For a two-dimensional linear elasticity problem, a CR finite element was introduced to overcome the locking phenomenon in [9]. The corresponding three-dimensional case was addressed in [47]. More recently, a robust CR element was presented to solve non-stationary elastic vibration problems [20]. Some developments of CR elements for various application problems can be found in the review article [7]. In the context of nonconforming finite elements for the Biot problem, coupling of nonconforming and mixed finite element methods were investigated in [27,36,54]. Our method is different from [27], because the method therein is based on a three-field formulation, while our method is based on a two-field formulation, and therefore fewer variables are involved.

The rest of this article is organized as follows. In the next section, we introduce the Biot consolidation model and its weak formulation. In Section 3, we provide a fully mixed FEM with backward Euler time-stepping for the Biot equation. The well-posedness of our numerical scheme is studied in Section 4. Under certain regularity assumptions on the weak solutions, we derive an optimal-order a priori error estimates in Section 5. Some numerical experiments are presented in Section 6 to support our theory. Concluding remarks are made in Section 7.

2. The Biot Consolidation Problem

Let $\Omega \subset \mathbb{R}^d$, $d = 2, 3$ be a simply connected bounded convex polygonal or polyhedral domain with a Lipschitz boundary $\partial\Omega$. We consider the following quasi-static Biot consolidation model in Ω over a time interval $(0, T]$ as follows [41,48]:

$$-\nabla \cdot \boldsymbol{\sigma} + \alpha \nabla p = \boldsymbol{f} \qquad \text{in } \Omega \times (0, T], \tag{2.1}$$

$$-c_0 \partial_t p - \alpha \nabla \cdot \partial_t \boldsymbol{u} + \nabla \cdot (\boldsymbol{K} \nabla p) = g \quad \text{in } \Omega \times (0, T]. \tag{2.2}$$

Here, $\boldsymbol{u}(x, t)$ is the displacement of the solid phase, $p(x, t)$ is the fluid pressure, $\boldsymbol{\sigma}(x, t)$ denotes the elasticity stress tensor

$$\boldsymbol{\sigma} = \lambda \mathrm{tr}\big(\boldsymbol{\epsilon}(\boldsymbol{u})\big)\boldsymbol{I} + 2\mu\boldsymbol{\epsilon}(\boldsymbol{u}) \quad \text{with} \quad \boldsymbol{\epsilon}(\boldsymbol{u}) = \frac{1}{2}\big(\nabla \boldsymbol{u} + (\nabla \boldsymbol{u})^T\big)$$

and $\boldsymbol{I} \in \mathbb{R}^{d\times d}$ is identity matrix, $\lambda > 0$ and $\mu > 0$ are the Lamé constants which are given by

$$\lambda = \frac{E\nu}{(1+\nu)(1-2\nu)}, \quad \mu = \frac{E\nu}{2(1+\nu)} \tag{2.3}$$

with E being the Young's modulus and ν being the Poisson's ratio, $c_0 \geq 0$ is the storage coefficient, $\alpha > 0$ is the Biot-Willis constant which is assumed to be 1 in this work, g is a source term, $\boldsymbol{f}$ stands for the external force, $\boldsymbol{K}(x) \in \mathbb{R}^{d\times d}$ is a symmetric and uniformly positive definite tensor satisfying

$$k_{\min}\boldsymbol{\xi}^T\boldsymbol{\xi} \leq \boldsymbol{\xi}^T\boldsymbol{K}(x)\boldsymbol{\xi} \leq k_{\max}\boldsymbol{\xi}^T\boldsymbol{\xi}, \quad \forall \boldsymbol{\xi} \in \mathbb{R}^d,$$

where $k_{\min}$ and $k_{\max}$ are two positive constants.

The boundary conditions for the Biot system (2.1)-(2.2) read as

$$\boldsymbol{u} = 0 \quad \text{and} \quad \boldsymbol{K}\nabla p \cdot \boldsymbol{n} = 0 \quad \text{on } \Gamma_c \times (0, T], \tag{2.4}$$

$$\boldsymbol{\sigma} \cdot \boldsymbol{n} = \boldsymbol{\beta} \quad \text{and} \quad p = 0 \quad \text{on } \Gamma_t \times (0, T]. \tag{2.5}$$

Here, $\partial\Omega = \Gamma_c \cup \Gamma_t$, $\Gamma_c \cap \Gamma_t = \emptyset$ with $|\Gamma_c| > 0$ and $|\Gamma_t| > 0$, $\boldsymbol{n}$ is the unit outward normal vector. Additionally, the initial conditions are given by

$$\boldsymbol{u}(x, 0) = \boldsymbol{u}^0, \quad p(x, 0) = p^0. \tag{2.6}$$

In order to state the weak formulation of (2.1)-(2.2), we introduce the standard Sobolev space $H^m(\mathcal{D})$ with regularity exponent $m \geq 0$. The corresponding norm and the semi-norm are denoted as $\|\cdot\|_{m,\mathcal{D}}$ and $|\cdot|_{m,\mathcal{D}}$. When $m=0$, $H^0(\mathcal{D})$ is reduced to $L^2(\mathcal{D})$, and we denote its inner product by $(\cdot,\cdot)_D$. For simplicity, when $\mathcal{D}=\Omega$, we will omit the index Ω. For the space $\boldsymbol{H}^m(\mathcal{D}) = [H^m(\mathcal{D})]^d$, its norm is still denoted by $\|\cdot\|_{m,\mathcal{D}}$. A subspace of $H^1(\Omega)$ with vanishing trace on Γ is denoted by $H^1_{0,\Gamma}(\Omega) := \{v \in H^1(\Omega) : v|_\Gamma = 0\}$. For ease of notations, we set $\boldsymbol{V} = [H^1_{0,\Gamma_c}(\Omega)]^d$ and $Q = \mathrm{H}_{0,\Gamma_t}(\Omega)$.

After integrating by parts, we obtain the standard mixed weak formulation of (2.1)-(2.2): Find $(\boldsymbol{u},p) \in \boldsymbol{V} \times Q$ such that $t \in (0,T]$,

$$a_{\boldsymbol{u}}(\boldsymbol{u},\boldsymbol{v}) - b(\boldsymbol{v},p) = (\boldsymbol{f},\boldsymbol{v}) + \langle \boldsymbol{\beta},\boldsymbol{v}\rangle_{\Gamma_t}, \qquad \forall \boldsymbol{v} \in \boldsymbol{V}, \tag{2.7}$$

$$-(c_0\partial_t p,q) - b(\partial_t \boldsymbol{u},q) - a_p(p,q) = (g,q), \quad \forall q \in Q, \tag{2.8}$$

where

$$\begin{aligned} a_{\boldsymbol{u}}(\boldsymbol{u},\boldsymbol{v}) &= 2\mu \int_\Omega \boldsymbol{\epsilon}(\boldsymbol{u}) : \boldsymbol{\epsilon}(\boldsymbol{v}) dx + \lambda \int_\Omega \nabla\cdot\boldsymbol{u}\nabla\cdot\boldsymbol{v} dx, \\ a_p(p,q) &= \int_\Omega \boldsymbol{K}\nabla p\cdot\nabla q dx, \\ b(\boldsymbol{v},q) &= \int_\Omega \nabla\cdot\boldsymbol{v} q dx. \end{aligned}$$

The well-posedness of the continuous variational problem (2.7)-(2.8) can be found in [49].

In the sequel, we shall deal with the functions of time and space. To this end, we introduce the standard Bochner space $L^p(0,T;H^m(\Omega))$, which consists of all functions $u : [0,T] \to H^m(\Omega)$ with norm

$$\|u\|_{L^p(0,T;H^m(\Omega))} := \left(\int_0^T \|u(t)\|_m^p dt\right)^{\frac{1}{p}}$$

for $1 \leq p < \infty$. When $p = \infty$, the space $L^\infty(0,T;H^m(\Omega))$ is endowed with the norm

$$\|u\|_{L^\infty(0,T;H^m(\Omega))} := \sup_{0\leq t\leq T} \|u(t)\|_m.$$

3. The Mixed Finite Element Method

In this section, we shall provide a mixed finite element scheme to solve (2.1)-(2.2). For ease of presentation, we only consider the numerical method for the problem in two dimensions. The extension to the three dimension case and the corresponding analysis can be obtained straightforwardly by using the results in [34] and the analysis here. Let $\mathcal{T}_h = \{K\}$ be a shape-regular triangulation of Ω. We denote h_K as the diameter of K and $h = \max_{K\in\mathcal{T}_h} h_K$. Moreover, we denote $\mathcal{E}_h^I$ as the set of interior edges of elements in $\mathcal{T}_h$, $\mathcal{E}_h^c$ as the set of boundary edges on Γ_c, and $\mathcal{E}_h^t$ as the set of boundary edges on Γ_t. Hence, the set of all edges $\mathcal{E}_h = \mathcal{E}_h^I \cup \mathcal{E}_h^c \cup \mathcal{E}_h^t$. h_e is used to denote the length of an edge $e \in \mathcal{E}_h$, and the set $\mathcal{E}_h^K = \{e \in \mathcal{E}_h \,|\, e \subset \partial K\}$.

For approximating the displacement, we introduce the nonconforming Crouzeix-Raviart $\mathbb{P}_1$ finite element space [15]

$$\boldsymbol{V}_h := \left\{\boldsymbol{v}_h \in \boldsymbol{L}^2(\Omega) : \boldsymbol{v}_h|_K \in [\mathbb{P}_1(K)]^2,\ \int_e [\boldsymbol{v}_h]_e d_F = 0,\ \forall e \in \mathcal{E}_h^I \text{ and } \int_e \boldsymbol{v}_h d_F = 0,\ \forall e \in \mathcal{E}_h^c\right\},$$

where $[\boldsymbol{v}_h]_e$ is the jump of the function $\boldsymbol{v}_h$ across an edge e, and $\mathbb{P}_1(K)$ refers to the space of polynomials of total degree ≤ 1 on K. For approximating the fluid pressure, we apply the conforming $\mathbb{P}_1$ finite element space

$$Q_h := \big\{q_h \in C^0(\bar{\Omega}) \cap H^1_{0,\Gamma_t}(\Omega) : q_h|_K \in \mathbb{P}_1(K)\big\}.$$

For the time discretization, we use a uniform mesh for an interval $[0,T]$ with a time step $\Delta t = T/N$. For any function $\psi(t,x)$, at each time $t^n = n\Delta t$, $n = 1,\dots,N$, we denote $\psi^n = \psi(t^n, x)$, $\forall x \in \Omega$.

The fully discrete scheme for the Biot model (2.1)-(2.2) with the backward Euler scheme in time reads as: Find $(u_h^n, p_h^n) \in \boldsymbol{V}_h \times Q_h$ such that

$$a_h^{\boldsymbol{u}}(\boldsymbol{u}_h^n, \boldsymbol{v}_h) - b_h(\boldsymbol{v}_h, p_h^n) = (\boldsymbol{f}^n, \boldsymbol{v}_h) + \langle \boldsymbol{\beta}^n, \boldsymbol{v}_h\rangle_{\Gamma_t}, \qquad \forall \boldsymbol{v}_h \in \boldsymbol{V}_h, \tag{3.1}$$

$$-(c_0\bar{\partial}_t p_h^n, q_h) - b_h(\bar{\partial}_t \boldsymbol{u}_h^n, q_h) - a_h^p(p_h^n, q_h) = (g^n, q_h), \quad \forall q_h \in Q_h, \tag{3.2}$$

where

$$\bar{\partial}_t p_h^n = \frac{p_h^n - p_h^{n-1}}{\Delta t}, \quad \bar{\partial}_t \boldsymbol{u}_h^n = \frac{\boldsymbol{u}_h^n - \boldsymbol{u}_h^{n-1}}{\Delta t},$$

and

$$\begin{aligned}
a_h^{\boldsymbol{u}}(\boldsymbol{u}_h, \boldsymbol{v}_h) &= 2\mu \sum_{K\in\mathcal{T}_h} \int_K \boldsymbol{\epsilon}(\boldsymbol{u}_h) : \boldsymbol{\epsilon}(\boldsymbol{v}_h) dx + \lambda \sum_{K\in\mathcal{T}_h} \int_K \nabla\cdot \boldsymbol{u}_h \nabla\cdot \boldsymbol{v}_h dx \\
&\quad + 2\mu\gamma \sum_{e\in\mathcal{E}_h} h_e^{-1} \int_e [\boldsymbol{u}_h]\cdot[\boldsymbol{v}_h] d_F, \\
a_h^p(p_h, q_h) &= \int_\Omega \boldsymbol{K}\nabla p_h \cdot \nabla q_h dx, \\
b_h(\boldsymbol{v}_h, q_h) &= (\nabla_h\cdot \boldsymbol{v}_h, q_h) =: \sum_{K\in\mathcal{T}_h} \int_K \nabla\cdot \boldsymbol{v}_h q_h dx.
\end{aligned}$$

The stabilization term $2\mu\gamma\sum_{e\in\mathcal{E}_h} h_e^{-1}\int_e [\boldsymbol{u}_h]\cdot[\boldsymbol{v}_h]d_F$ in $a_h^{\boldsymbol{u}}(\boldsymbol{u}_h,\boldsymbol{v}_h)$ suggested by [22] is used to satisfy the discrete Korn's inequality. More details on the properties of Korn's inequality can be found in [6]. In practical computations, the stabilization parameter can be set as $\gamma = 1/2$ (see [22]).

In petroleum engineering, one can enforce an initial pressure distribution, and then compute an estimated initial displacement from Eq. (2.1). More precisely, we first set $p_h^0 := p_I^0$ as the elliptic projection of p^0, that is,

$$a_h^p(p_I^0, q_h) = a_h^p(p^0, q_h), \quad \forall q_h \in Q_h, \tag{3.3}$$

and then let $\boldsymbol{u}_h^0 := \boldsymbol{u}_I^0$ be the solution of

$$a_h^{\boldsymbol{u}}(\boldsymbol{u}_I^0, \boldsymbol{v}_h) = (\boldsymbol{f}^0, \boldsymbol{v}_h) + (\boldsymbol{\beta}^0, \boldsymbol{v}_h)_{\Gamma_t} - b_h(\boldsymbol{v}_h, p_I^0), \quad \forall \boldsymbol{v}_h \in \boldsymbol{V}_h. \tag{3.4}$$

When the permeability and/or time steps are small, there will be nonphysical pressure oscillations in numerical approximations. Inspired by [48], in order to avoid nonphysical pressure oscillations in the pore fluid pressure, we can add a stabilization term

$$B_{stab}(\rho,\eta) = \frac{\varepsilon h^2}{\lambda + 2\mu} \int_\Omega \nabla\bar{\partial}_t\rho \cdot \nabla\eta dx \tag{3.5}$$

in Eq. (3.2). More precisely, it results in the following discrete scheme: Find $(u_h^n, p_h^n) \in \boldsymbol{V}_h \times Q_h$ such that

$$
a_h^{\boldsymbol{u}}(\boldsymbol{u}_h^n, \boldsymbol{v}_h) - b_h(\boldsymbol{v}_h, p_h^n) = (\boldsymbol{f}^n, \boldsymbol{v}_h) + \langle \boldsymbol{\beta}^n, \boldsymbol{v}_h \rangle_{\Gamma_t}, \qquad \forall \boldsymbol{v}_h \in \boldsymbol{V}_h, \tag{3.6}
$$

$$
-(c_0 \bar{\partial}_t p_h^n, q_h) - b_h(\bar{\partial}_t \boldsymbol{u}_h^n, q_h) - a_h^p(p_h^n, q_h) - B_{stab}(p_h^n, q_h) = (g^n, q_h), \quad \forall q_h \in Q_h. \tag{3.7}
$$

In this work, we take $\varepsilon = 1/4$ as suggested in [48].

Remark 3.1. In this paper, we consider mixed boundary conditions, in particular, we assume that $\Gamma_t \neq \varnothing$. When $\Gamma_t = \varnothing$, one needs to deal with the pure traction problem. For the pure traction boundary problem, Falk in [18] has proposed a stable CR element that relies on the projection onto the macro element. We refer readers to [18] to see more details.

Remark 3.2. The authors in [22] suggested that the stabilization term includes all the edges. Later, in [6] it is pointed that, only interior edges $\mathcal{E}_h^I$ and boundary edges $\mathcal{E}_h^t$ on Γ_t are needed to satisfy the discrete Korn's inequality. More recently, in [39], it is proved that the jumps can be replaced with only the normal component of jumps.

Remark 3.3. Motivated by [48], we have utilized a stabilization term $B_{stab}(p_h^n, q_h)$ to remove nonphysical pressure oscillations. The finite element pair we used indeed satisfies the inf-sup condition (see Lemma 4.1 below). However, in [2, 48], it is pointed out that in two-field formulation, the inf-sup condition is not a sufficient condition to avoid pressure oscillations, a remedy for this is to add a time-dependent stabilization term $B_{stab}(p_h^n, q_h)$. Moreover, in [48], it is also shown that this instability may arise from the lack of monotonicity of discrete schemes. In the three-field formulation, in [24], it is proved that when the finite element pairs satisfy some suitable inf-sup conditions, one can obtain a family of parameter-robust numerical schemes.

4. Well-Posedness

This section is devoted to the well-posedness of the discrete schemes (3.1)-(3.2). From (3.1)-(3.2), we can see that, at each time step, we need solve the following linear system: Find $\boldsymbol{u}_h^n \in \boldsymbol{V}_h$ and $q_h^n \in Q_h$ such that

$$
a_h^{\boldsymbol{u}}(\boldsymbol{u}_h^n, \boldsymbol{v}_h) - b_h(\boldsymbol{v}_h, p_h^n) = (\boldsymbol{f}^n, \boldsymbol{v}_h) + \langle \boldsymbol{\beta}^n, \boldsymbol{v}_h \rangle_{\Gamma_c}, \quad \forall \boldsymbol{v}_h \in \boldsymbol{V}_h, \tag{4.1}
$$

$$
-(c_0 p_h^n, q_h) - b_h(\boldsymbol{u}_h^n, q_h) - \Delta t a_h^p(p_h^n, q_h) = (\tilde{g}^n, q_h), \quad \forall q_h \in Q_h. \tag{4.2}
$$

Here, $\tilde{g}^n = \Delta t g^n - \nabla_h \cdot \boldsymbol{u}_h^{n-1} - c_0 p_h^{n-1}$. Next, we shall prove the well-posedness of (4.1)-(4.2), which is equivalent to that of (3.1)-(3.2).

First, we define the following norms on $\boldsymbol{v} \in \boldsymbol{V} + \boldsymbol{V}_h$ and $q \in Q + Q_h$:

$$
\|\boldsymbol{v}\|_{\boldsymbol{V}}^2 = a_h^{\boldsymbol{u}}(\boldsymbol{v}, \boldsymbol{v}), \quad \|q\|_Q^2 = a_h^p(q, q). \tag{4.3}
$$

It is easy to check that

$$
a_h^{\boldsymbol{u}}(\boldsymbol{w}, \boldsymbol{v}) \le \|\boldsymbol{w}\|_{\boldsymbol{V}} \|\boldsymbol{v}\|_{\boldsymbol{V}}, \tag{4.4}
$$

$$
b_h(\boldsymbol{v}, q) \le C \|\boldsymbol{v}\|_{\boldsymbol{V}} \|q\|_0. \tag{4.5}
$$

Then, we have the following inf-sup condition.

Lemma 4.1. *It holds that*

$$\sup_{\boldsymbol{v}_h\in\boldsymbol{V}_h}\frac{b_h(\boldsymbol{v}_h,q_h)}{\|\boldsymbol{v}_h\|_{\boldsymbol{V}}}\geq\alpha_0\|q_h\|_0 \tag{4.6}$$

for all $q_h\in Q_h$.

Proof. The detailed proof of this result is provided in [34, Theorem 3]. □

Inspired by [26], we define a bilinear form for $\boldsymbol{u}_h,\boldsymbol{v}_h\in\boldsymbol{V}_h$ and $p_h,q_h\in Q_h$ by

$$\mathbb{B}_h(\boldsymbol{u}_h,p_h;\boldsymbol{v}_h,q_h)=a_h^{\boldsymbol{u}}(\boldsymbol{u}_h,\boldsymbol{v}_h)-b_h(\boldsymbol{v}_h,p_h)-b_h(\boldsymbol{u}_h,q_h)-\Delta t a_h^p(p_h,q_h)-(c_0p_h,q_h),$$

and the weighted norm by

$$|||(\boldsymbol{v}_h,q_h)|||_{\Delta t}=\left(\|\boldsymbol{v}_h\|_{\boldsymbol{V}}^2+\|q_h\|_0^2+\Delta t\|q_h\|_Q^2\right)^{\frac{1}{2}}. \tag{4.7}$$

Now, we are in a position to state the main result of this subsection. By using the theoretical framework stated in [48] and Lemma 4.1, we obtain the following well-posedness result.

Theorem 4.1. *It holds that*

$$\sup_{(\boldsymbol{v}_h,q_h)\in\boldsymbol{V}_h\times Q_h}\frac{\mathbb{B}_h(\boldsymbol{u}_h,p_h;\boldsymbol{v}_h,q_h)}{|||(\boldsymbol{v}_h,q_h)|||_{\Delta t}}\geq\beta_0|||(\boldsymbol{u}_h,p_h)|||_{\Delta t}, \tag{4.8}$$

which implies that the discrete linear system (4.1)-(4.2) *is well-posed.*

5. Error Estimates

In this section, we shall give the detailed a priori error estimates for the fully finite element scheme (3.1)-(3.2). First, we recall the regularity results for the displacement $\boldsymbol{u}$ (see [55, Theorem 3.3]).

Theorem 5.1. *Let* $(\boldsymbol{u},p)$ *be the solutions of* (2.1)-(2.2), *it holds*

$$\begin{aligned}&\sup_{0\leq t\leq T}\|\boldsymbol{u}(t)\|_2+\sup_{0\leq t\leq T}\lambda\|\nabla\cdot\boldsymbol{u}(t)\|_1\\&\leq C\bigg\{\|p^0\|_1+\sup_{0\leq t\leq T}\|\boldsymbol{f}(t)\|_0+\sup_{0\leq t\leq T}\|g(t)\|_0\\&\qquad+\left(\int_0^T\|\partial_t\boldsymbol{f}(s)\|_{-1}^2ds\right)^{\frac{1}{2}}+\left(\int_0^T\|\partial_t g(s)\|_0^2ds\right)^{\frac{1}{2}}\bigg\},\end{aligned} \tag{5.1}$$

where $C>0$ *is a constant depending on the parameter* μ, *but independent of* λ.

Remark 5.1. In light of [55, Remark 3.4], when the time derivatives of solution and the right-hand sides of problems (2.1)-(2.2) are smooth enough, similar regularity results are also valid for $\partial_t\boldsymbol{u}$ and $\partial_{tt}\boldsymbol{u}$.

In addition, for the pressure p, we have the following regularity result.

Theorem 5.2. *Let* $(\boldsymbol{u},p)$ *be the solutions of* (2.1)-(2.2), *there holds*

$$\begin{aligned}\sup_{0\leq t\leq T}\|p(t)\|_2\leq C\bigg\{&\|p^0\|_2+\left(\int_0^T\|g(s)\|_0^2ds\right)^{\frac{1}{2}}+\left(\int_0^T\|\partial_t g(s)\|_0^2ds\right)^{\frac{1}{2}}\\&+\left(\int_0^T\|\nabla\cdot\partial_t\boldsymbol{u}(s)\|_0^2ds\right)^{\frac{1}{2}}+\left(\int_0^T\|\nabla\cdot\partial_{tt}\boldsymbol{u}(s)\|_0^2ds\right)^{\frac{1}{2}}\bigg\},\end{aligned} \tag{5.2}$$

where $C>0$ *is a constant depending on the parameter* μ, *but independent of* λ.

Proof. It follows from (2.2) that

$$c_0\partial_t p - \nabla\cdot(\boldsymbol{K}\nabla p) = -g - \alpha\nabla\cdot\partial_t\boldsymbol{u} \quad \text{in } \Omega\times(0,T]. \tag{5.3}$$

From the left-hand side, we see that this is a parabolic equation for p, the standard regularity result implies that (see [17, Theorem 5, Chapter 7])

$$\begin{aligned}
\sup_{0\le t\le T}\|p(t)\|_2 \le C\Bigg\{&\|p^0\|_2 + \Big(\int_0^T \|g(s)\|_0^2 ds\Big)^{\frac12} + \Big(\int_0^T \|\partial_t g(s)\|_0^2 ds\Big)^{\frac12} \\
&+ \Big(\int_0^T \|\alpha\nabla\cdot\partial_t\boldsymbol{u}(s)\|_0^2 ds\Big)^{\frac12} + \Big(\int_0^T \|\alpha\nabla\cdot\partial_{tt}\boldsymbol{u}(s)\|_0^2 ds\Big)^{\frac12}\Bigg\} \\
\le C\Bigg\{&\|p^0\|_2 + \Big(\int_0^T \|g(s)\|_0^2 ds\Big)^{\frac12} + \Big(\int_0^T \|\partial_t g(s)\|_0^2 ds\Big)^{\frac12} \\
&+ \Big(\int_0^T \|\nabla\cdot\partial_t\boldsymbol{u}(s)\|_0^2 ds\Big)^{\frac12} + \Big(\int_0^T \|\nabla\cdot\partial_{tt}\boldsymbol{u}(s)\|_0^2 ds\Big)^{\frac12}\Bigg\},
\end{aligned}$$

which is the desired estimate. □

Remark 5.2. From Remark 5.1, we see that the term $(\int_0^T \|\nabla\cdot\partial_t\boldsymbol{u}(s)\|_0^2 ds)^{1/2} + (\int_0^T \|\nabla\cdot\partial_{tt}\boldsymbol{u}(s)\|_0^2 ds)^{1/2}$ in (5.2) can be bounded by suitable norms of $\boldsymbol{f}$ and g, and initial conditions of p. This implies that $\sup_{0\le t\le T}\|p(t)\|_2 \le C$ with C independent of λ. When the time derivatives of solution and the right-hand sides of problems (2.1)-(2.2) are smooth enough, similar results are also valid for $\partial_t p$ and $\partial_{tt} p$.

5.1. Error estimates for $c_0 = 0$

Similar to the treatment for the initial conditions as stated in (3.3)-(3.4), we begin by defining the following projections $p_I^n \in Q_h$ and $\boldsymbol{u}_I^n \in \boldsymbol{V}_h$:

$$a_h^p(p_I^n, q_h) = a_h^p(p^n, q_h), \qquad \forall q_h \in Q_h, \tag{5.4}$$
$$a_h^{\boldsymbol{u}}(\boldsymbol{u}_I^n, \boldsymbol{v}_h) = (\boldsymbol{f}^n, \boldsymbol{v}_h) + \langle\boldsymbol{\beta}^n, \boldsymbol{v}_h\rangle_{\Gamma_t} - b_h(\boldsymbol{v}_h, p_I^n), \quad \forall \boldsymbol{v}_h \in \boldsymbol{V}_h. \tag{5.5}$$

Moreover, we define the Crouzeix-Raviart interpolation operator $\Pi_K : [H^1(K)]^2 \to [\mathbb{P}_1(K)]^2$ by (see [15])

$$\int_e \Pi_K \boldsymbol{v} d_F = \int_e \boldsymbol{v} d_F, \quad \forall e \in \mathcal{E}_h^K.$$

Then, the global Crouzeix-Raviart interpolation operator $\Pi_h : \boldsymbol{H}^1(\Omega) \to \boldsymbol{V}_h$ can be constructed by

$$(\Pi_h \boldsymbol{v})|_K = \Pi_K(\boldsymbol{v}|_K), \quad \forall K \in \mathcal{T}_h. \tag{5.6}$$

It is well known that the following estimate holds (see [22, Lemma 2.4]):

$$\|\boldsymbol{v} - \Pi_h\boldsymbol{v}\|_{\boldsymbol{V}} \le Ch\big((2\mu)^{\frac12}\|\boldsymbol{v}\|_2 + \lambda^{\frac12}\|\nabla\cdot\boldsymbol{v}\|_1\big). \tag{5.7}$$

Based on the above notations and results, we obtain the following useful approximation properties for p_I^n and $\boldsymbol{u}_I^n$.

Lemma 5.1. *Assume that $p^n \in H^2(\Omega)$ for $1 \le n \le N$, for p_I^n given by (5.5) there holds*

$$\|p^n - p_I^n\|_Q \le Ch\|p^n\|_2, \tag{5.8}$$

$$\|p^n - p_I^n\|_0 \le Ch^2\|p^n\|_2. \tag{5.9}$$

Moreover, assume that $\boldsymbol{u}^n \in \boldsymbol{H}^2(\Omega)$ and $\nabla\cdot\boldsymbol{u}^n \in H^1(\Omega)$, for $\boldsymbol{u}_I^n$ given by (5.4), we have

$$\|\boldsymbol{u}^n - \boldsymbol{u}_I^n\|_{\boldsymbol{V}} \le Ch\big((2\mu)^{\frac{1}{2}}\|\boldsymbol{u}^n\|_2 + \lambda^{\frac{1}{2}}\|\nabla\cdot\boldsymbol{u}^n\|_1 + \|p^n\|_2\big). \tag{5.10}$$

Proof. (1) Proof of (5.8). The definition of p_I^n in (5.4) implies that

$$\|p^n - p_I^n\|_Q = \inf_{q_h\in Q_h}\|p^n - q_h\|_Q. \tag{5.11}$$

We then obtain the estimate (5.8) by the standard finite element approximate properties (see [8]).

(2) Proof of (5.9). The desired estimate (5.9) can be obtained by combining (5.8) and a duality argument. We refer [5, Theorem 3.2] for more details.

(3) Proof of (5.10). We first split $\boldsymbol{u}^n - \boldsymbol{u}_I^n = \boldsymbol{u}^n - \Pi_h\boldsymbol{u}^n + \Pi_h\boldsymbol{u}^n - \boldsymbol{u}_I^n$. The term $\Pi_h\boldsymbol{u}^n - \boldsymbol{u}_I^n$ satisfies

$$\|\Pi_h\boldsymbol{u}^n - \boldsymbol{u}_I^n\|_{\boldsymbol{V}} = \sup_{\boldsymbol{v}_h\in\boldsymbol{V}_h}\frac{a_h^{\boldsymbol{u}}(\Pi_h\boldsymbol{u}^n - \boldsymbol{u}_I^n, \boldsymbol{v}_h)}{\|\boldsymbol{v}_h\|_{\boldsymbol{V}}}. \tag{5.12}$$

Recalling $\boldsymbol{f}^n = -\nabla\cdot\boldsymbol{\sigma}^n + \nabla p^n$, and using (5.5), we have

$$\begin{aligned}
a_h^{\boldsymbol{u}}(\Pi_h\boldsymbol{u}^n - \boldsymbol{u}_I^n, \boldsymbol{v}_h) &= a_h^{\boldsymbol{u}}(\Pi_h\boldsymbol{u}^n, \boldsymbol{v}_h) - (\boldsymbol{f}^n, \boldsymbol{v}_h) - \langle\boldsymbol{\beta}^n, \boldsymbol{v}_h\rangle_{\Gamma_t} + b_h(\boldsymbol{v}_h, p_I^n)\\
&= \big(a_h^{\boldsymbol{u}}(\Pi_h\boldsymbol{u}^n, \boldsymbol{v}_h) + (\nabla\cdot\boldsymbol{\sigma}^n, \boldsymbol{v}_h)\big) + \big(b_h(\boldsymbol{v}_h, p_I^n) - (\nabla p^n, \boldsymbol{v}_h)\big)\\
&\equiv \mathbb{D}_1 + \mathbb{D}_2.
\end{aligned} \tag{5.13}$$

Integrating by parts, we can estimate the first term $\mathbb{D}_1$ as follows:

$$\begin{aligned}
\mathbb{D}_1 &= a_h^{\boldsymbol{u}}(\Pi_h\boldsymbol{u}^n - \boldsymbol{u}^n, \boldsymbol{v}_h) + \sum_{K\in\mathcal{T}_h}\sum_{e\in\partial K\setminus\Gamma_t}\langle\boldsymbol{\sigma}^n\boldsymbol{n}_K, \boldsymbol{v_h}\rangle_e\\
&= a_h^{\boldsymbol{u}}(\Pi_h\boldsymbol{u}^n - \boldsymbol{u}^n, \boldsymbol{v}_h) + \sum_{K\in\mathcal{T}_h}\sum_{e\in\partial K\setminus\Gamma_t}2\mu\langle\epsilon(\boldsymbol{u}^n)\boldsymbol{n}_K, \boldsymbol{v_h}\rangle_e\\
&\quad+\sum_{K\in\mathcal{T}_h}\sum_{e\in\partial K\setminus\Gamma_t}\lambda\langle(\nabla\cdot\boldsymbol{u}^n)\boldsymbol{n}_K, \boldsymbol{v_h}\rangle_e\\
&= a_h^{\boldsymbol{u}}(\Pi_h\boldsymbol{u}^n - \boldsymbol{u}^n, \boldsymbol{v}_h) + \sum_{K\in\mathcal{T}_h}\sum_{e\in\partial K\setminus\Gamma_t}2\mu\big\langle\big(\epsilon(\boldsymbol{u}^n) - \overline{\epsilon(\boldsymbol{u}^n)}\big)\boldsymbol{n}_K, \boldsymbol{v_h} - \overline{\boldsymbol{v_h}}\big\rangle_e\\
&\quad+\sum_{K\in\mathcal{T}_h}\sum_{e\in\partial K\setminus\Gamma_t}\lambda\langle(\nabla\cdot\boldsymbol{u}^n - \overline{\nabla\cdot\boldsymbol{u}^n})\boldsymbol{n}_K, \boldsymbol{v_h} - \overline{\boldsymbol{v_h}}\rangle_e\\
&\le \|\Pi_h\boldsymbol{u}^n - \boldsymbol{u}^n\|_{\boldsymbol{V}}\|\boldsymbol{v}_h\|_{\boldsymbol{V}} + \sum_{K\in\mathcal{T}_h}\sum_{e\in\partial K\setminus\Gamma_t}2\mu\|\epsilon(\boldsymbol{u}^n) - \overline{\epsilon(\boldsymbol{u}^n)}\|_{0,e}\|\boldsymbol{v_h} - \overline{\boldsymbol{v_h}}\|_{0,e}\\
&\quad+\sum_{K\in\mathcal{T}_h}\sum_{e\in\partial K\setminus\Gamma_t}\lambda\|\nabla\cdot(\boldsymbol{u}^n) - \overline{\nabla\cdot(\boldsymbol{u}^n)}\|_{0,e}\|\boldsymbol{v_h} - \overline{\boldsymbol{v_h}}\|_{0,e}\\
&\le \|\Pi_h\boldsymbol{u}^n - \boldsymbol{u}^n\|_{\boldsymbol{V}}\|\boldsymbol{v}_h\|_{\boldsymbol{V}} + C\sum_{K\in\mathcal{T}_h}2\mu h_K^{\frac{1}{2}}|\boldsymbol{u}^n|_{2,K}\,h_K^{\frac{1}{2}}|\boldsymbol{v_h}|_{1,K}\\
&\quad+C\sum_{K\in\mathcal{T}_h}2\lambda h_K^{\frac{1}{2}}|\nabla\cdot\boldsymbol{u}^n|_{1,K}\,h_K^{\frac{1}{2}}|\boldsymbol{v_h}|_{1,K}
\end{aligned}$$

$$
\begin{aligned}
&\le \|\Pi_h \boldsymbol{u}^n - \boldsymbol{u}^n\|_{\boldsymbol{V}} \|\boldsymbol{v}_h\|_{\boldsymbol{V}} + Ch\Big(\sum_{K\in\mathcal{T}_h} (2\mu|\boldsymbol{u}^n|_{2,K} + \lambda|\nabla\cdot\boldsymbol{u}^n|_{1,K})^2\Big)^{\frac{1}{2}} \Big(\sum_{K\in\mathcal{T}_h} |\boldsymbol{v_h}|^2_{1,K}\Big)^{\frac{1}{2}} \\
&\le \|\Pi_h \boldsymbol{u}^n - \boldsymbol{u}^n\|_{\boldsymbol{V}} \|\boldsymbol{v}_h\|_{\boldsymbol{V}} + Ch\big(2\mu|\boldsymbol{u}^n|_2 + \lambda|\nabla\cdot\boldsymbol{u}^n|_1\big)|\boldsymbol{v}_h|_{1,h} \\
&\le \|\Pi_h \boldsymbol{u}^n - \boldsymbol{u}^n\|_{\boldsymbol{V}} \|\boldsymbol{v}_h\|_{\boldsymbol{V}} + Ch\big(2\mu|\boldsymbol{u}^n|_2 + \lambda|\nabla\cdot\boldsymbol{u}^n|_1\big)\|\boldsymbol{v}_h\|_{\boldsymbol{V}},
\end{aligned}
\tag{5.14}
$$

where $\boldsymbol{n}_K$ denotes the outer unit normal to ∂K, $\bar{v}$ is the mean value of v on the edge e. Similarly, we can bound $\mathbb{D}_2$ by

$$
\begin{aligned}
\mathbb{D}_2 &= \sum_{K\in\mathcal{T}_h} (p_I^n - p^n, \nabla\cdot\boldsymbol{v}_h)_K + \sum_{K\in\mathcal{T}_h}\sum_{e\in\partial K\setminus\Gamma_t} \langle p^n \boldsymbol{n}_K, \boldsymbol{v}_h\rangle_e \\
&= \sum_{K\in\mathcal{T}_h} (p_I^n - p^n, \nabla\cdot\boldsymbol{v}_h)_K + \sum_{K\in\mathcal{T}_h}\sum_{e\in\partial K\setminus\Gamma_t} \langle (p^n - \overline{p^n})\boldsymbol{n}_K, \boldsymbol{v_h} - \overline{\boldsymbol{v_h}}\rangle_e \\
&\le \sum_{K\in\mathcal{T}_h} \|p_I^n - p^n\|_{0,K} \|\nabla\cdot\boldsymbol{v}_h\|_{0,K} + Ch|p^n|_1|\boldsymbol{v}_h|_{\boldsymbol{V}} \\
&\le Ch^2\|p^n\|_2\|\boldsymbol{v}_h\|_{1,h} + Ch|p^n|_1|\boldsymbol{v}_h|_{\boldsymbol{V}} \\
&\le Ch^2\|p^n\|_2\|\boldsymbol{v}_h\|_{\boldsymbol{V}} + Ch|p^n|_1|\boldsymbol{v}_h|_{\boldsymbol{V}}.
\end{aligned}
\tag{5.15}
$$

Combining (5.7) and (5.12)-(5.15), and using a triangle inequality, we obtain the desired estimate in (5.10). □

It follows from the Taylor's expansion that

$$
\frac{\phi^n - \phi^{n-1}}{\Delta t} = \partial_t\phi^n + \frac{1}{\Delta t}\int_{t^{n-1}}^{t^n} (t^{n-1} - s)\partial_{tt}\phi(s)ds \tag{5.16}
$$

with $\partial_t\phi^n := \partial_t\phi(t_n)$.

We are now in a position to state the following error estimates for $c_0 = 0$, which is the main result in this subsection.

Theorem 5.3. *Let $(\boldsymbol{u}, p) \in \boldsymbol{V}\times Q$ and $(\boldsymbol{u}_h^n, p_h^n) \in \boldsymbol{V}_h \times Q_h$ be the solutions of (2.1)-(2.2) and (3.1)-(3.2), respectively. Additionally, we assume that*

$$
\begin{aligned}
&\boldsymbol{u} \in L^\infty\big(0,T;\boldsymbol{H}^2(\Omega)\big), && \partial_t\boldsymbol{u} \in L^\infty\big(0,T;\boldsymbol{H}^2(\Omega)\big), && \partial_{tt}\boldsymbol{u} \in L^2\big(0,T;\boldsymbol{H}^2(\Omega)\big), \\
&\nabla\cdot(\partial_{tt}\boldsymbol{u}) \in L^2\big(0,T;L^2(\Omega)\big), && p \in L^\infty\big(0,T;H^2(\Omega)\big), && \partial_{tt}p \in L^2\big(0,T;H^2(\Omega)\big).
\end{aligned}
\tag{5.17}
$$

Then, we have the following error estimate:

$$
\max_{1\le n\le N} \|\boldsymbol{u}^n - \boldsymbol{u}_h^n\|^2_{\boldsymbol{V}} + \Delta t\sum_{n=1}^N \|p^n - p_h^n\|^2_Q \le C_{\mathrm{a}}\big(h^2\Phi_1 + (\Delta t)^2\Phi_2\big). \tag{5.18}
$$

Proof. Since the exact solutions $\boldsymbol{u}^n$ and p^n satisfy (2.1)-(2.2) at $t = t^n$, integrating by parts, using (5.16), we conclude that

$$
a_h^{\boldsymbol{u}}(\boldsymbol{u}^n, \boldsymbol{v}_h) - b_h(\boldsymbol{v}_h, p^n) = (\boldsymbol{f}^n, \boldsymbol{v}_h) + \sum_{K\in\mathcal{T}_h}\sum_{e\in\partial K\setminus\Gamma_t} \langle \boldsymbol{\sigma}^n\boldsymbol{n}_K, \boldsymbol{v}_h\rangle_e, \tag{5.19}
$$

$$
b_h(\bar{\partial}_t\boldsymbol{u}^n, q_h) + a_h^p(p^n, q_h) = (g^n, q_h) + \frac{1}{\Delta t}\Big(\int_{t^{n-1}}^{t^n} (t^{n-1} - s)\nabla\cdot(\partial_{tt}\boldsymbol{u})(s)ds, q_h\Big) \tag{5.20}
$$

for any $(\boldsymbol{v}_h, q_h) \in \boldsymbol{V}_h \times Q_h$. Subtracting (3.1) and (3.2) from (5.19) and (5.20), respectively, we have

$$a_h^{\boldsymbol{u}}(\boldsymbol{u}^n - \boldsymbol{u}_h^n, \boldsymbol{v}_h) - (p^n - p_h^n, \nabla_h \cdot \boldsymbol{v}_h) = \sum_{K\in\mathcal{T}_h} \sum_{e\in\partial K\backslash\Gamma_t} \langle \boldsymbol{\sigma}^n \boldsymbol{n}_K, \boldsymbol{v}_h\rangle_e, \tag{5.21}$$

$$\begin{aligned}&\left(\nabla_h \cdot \left(\frac{(\boldsymbol{u}^n - \boldsymbol{u}_h^n) - (\boldsymbol{u}^{n-1} - \boldsymbol{u}_h^{n-1})}{\Delta t}\right), q_h\right) + a_h^p(p^n - p_h^n, q_h)\\ &= \frac{1}{\Delta t}\left(\int_{t^{n-1}}^{t^n} (t^{n-1} - s)\nabla \cdot (\partial_{tt}\boldsymbol{u})(s)ds, q_h\right)\end{aligned} \tag{5.22}$$

for any $(\boldsymbol{v}_h, q_h) \in \boldsymbol{V}_h \times Q_h$.

We then split the error $p^n - p_h^n$ into $p^n - p_h^n = \xi_p^n + \theta_p^n$ with $\xi_p^n = p^n - p_I^n$ and $\theta_p^n = p_I^n - p_h^n$. Similarly, $\boldsymbol{u}^n - \boldsymbol{u}_h^n = \xi_{\boldsymbol{u}}^n + \theta_{\boldsymbol{u}}^n$ with $\xi_{\boldsymbol{u}}^n = \boldsymbol{u}^n - \boldsymbol{u}_I^n$ and $\theta_{\boldsymbol{u}}^n = \boldsymbol{u}_I^n - \boldsymbol{u}_h^n$. Since the estimates for ξ_p^n and $\xi_{\boldsymbol{u}}^n$ can be derived by the error bounds stated in (5.8)-(5.10), it remains to estimate θ_p^n and $\theta_{\boldsymbol{u}}^n$. Using (5.4), we have $a_h^p(\xi_p^n, \theta_p^n) = 0$, hence we can reformulate the expressions (5.21)-(5.22) by

$$\begin{aligned}&a_h^{\boldsymbol{u}}(\theta_{\boldsymbol{u}}^n, \boldsymbol{v}_h) - (\theta_p^n, \nabla_h \cdot \boldsymbol{v}_h)\\ &= -a_h^{\boldsymbol{u}}(\xi_{\boldsymbol{u}}^n, \boldsymbol{v}_h) + (\xi_p^n, \nabla_h \cdot \boldsymbol{v}_h) + \sum_{K\in\mathcal{T}_h} \sum_{e\in\partial K\backslash\Gamma_t} \langle \boldsymbol{\sigma}^n \boldsymbol{n}_K, \boldsymbol{v}_h\rangle_e,\end{aligned} \tag{5.23}$$

$$\begin{aligned}&\left(\nabla_h \cdot \left(\frac{\theta_{\boldsymbol{u}}^n - \theta_{\boldsymbol{u}}^{n-1}}{\Delta t}\right), q_h\right) + a_h^p(\theta_p^n, q_h)\\ &= -\left(\nabla_h \cdot \left(\frac{\xi_{\boldsymbol{u}}^n - \xi_{\boldsymbol{u}}^{n-1}}{\Delta t}\right), q_h\right) + \frac{1}{\Delta t}\left(\int_{t^{n-1}}^{t^n} (t^{n-1} - s)\nabla \cdot (\partial_{tt}\boldsymbol{u})(s)ds, q_h\right)\end{aligned} \tag{5.24}$$

for any $(\boldsymbol{v}_h, q_h) \in \boldsymbol{V}_h \times Q_h$. Setting $\boldsymbol{v}_h = (\theta_{\boldsymbol{u}}^n - \theta_{\boldsymbol{u}}^{n-1})/\Delta t$ and $q_h = \theta_p^n$ in (5.23)-(5.24) and adding them together, we obtain

$$\begin{aligned}a_h^{\boldsymbol{u}}(\theta_{\boldsymbol{u}}^n, \theta_{\boldsymbol{u}}^n) + \Delta t\|\theta_p^n\|_Q^2 &= a_h^{\boldsymbol{u}}(\theta_{\boldsymbol{u}}^n, \theta_{\boldsymbol{u}}^{n-1}) - a_h^{\boldsymbol{u}}(\xi_{\boldsymbol{u}}^n, \theta_{\boldsymbol{u}}^n - \theta_{\boldsymbol{u}}^{n-1}) + \big(\xi_p^n, \nabla_h \cdot (\theta_{\boldsymbol{u}}^n - \theta_{\boldsymbol{u}}^{n-1})\big)\\ &+ \sum_{K\in\mathcal{T}_h} \sum_{e\in\partial K\backslash\Gamma_t} \langle \boldsymbol{\sigma}^n \boldsymbol{n}_K, \theta_{\boldsymbol{u}}^n - \theta_{\boldsymbol{u}}^{n-1}\rangle_e - \big(\nabla_h \cdot (\xi_{\boldsymbol{u}}^n - \xi_{\boldsymbol{u}}^{n-1}), \theta_p^n\big)\\ &+ \left(\int_{t^{n-1}}^{t^n} (t^{n-1} - s)\nabla \cdot (\partial_{tt}\boldsymbol{u})(s)ds, \theta_p^n\right).\end{aligned} \tag{5.25}$$

Summing (5.25) from 1 to $m(\le N)$, noting that $\theta_{\boldsymbol{u}}^0 = 0$, and applying

$$a_h^{\boldsymbol{u}}\big(\theta_{\boldsymbol{u}}^n, \theta_{\boldsymbol{u}}^{n-1}\big) \le \frac{1}{2}\big(a_h^{\boldsymbol{u}}(\theta_{\boldsymbol{u}}^{n-1}, \theta_{\boldsymbol{u}}^{n-1}) + a_h^{\boldsymbol{u}}(\theta_{\boldsymbol{u}}^n, \theta_{\boldsymbol{u}}^n)\big) \tag{5.26}$$

to find that

$$\frac{1}{2}a_h^{\boldsymbol{u}}\big(\theta_{\boldsymbol{u}}^m, \theta_{\boldsymbol{u}}^m\big) + \Delta t\sum_{n=1}^m \|\theta_p^n\|_Q^2 \le \mathbb{T}_1 + \mathbb{T}_2 + \mathbb{T}_3 + \mathbb{T}_4 + \mathbb{T}_5, \tag{5.27}$$

where

$$\mathbb{T}_1 = -\sum_{n=1}^m a_h^{\boldsymbol{u}}\big(\xi_{\boldsymbol{u}}^n, \theta_{\boldsymbol{u}}^n - \theta_{\boldsymbol{u}}^{n-1}\big),$$

$$\mathbb{T}_2 = \sum_{n=1}^m \big(\xi_p^n, \nabla_h \cdot (\theta_{\boldsymbol{u}}^n - \theta_{\boldsymbol{u}}^{n-1})\big),$$

$$
\begin{aligned}
\mathbb{T}_3 &= \sum_{n=1}^{m} \sum_{K\in\mathcal{T}_h} \sum_{e\in\partial K\setminus\Gamma_t} \langle \boldsymbol{\sigma}^n \boldsymbol{n}_K, \theta_{\boldsymbol{u}}^n - \theta_{\boldsymbol{u}}^{n-1}\rangle_e,\\
\mathbb{T}_4 &= -\sum_{n=1}^{m} \big(\nabla_h \cdot (\xi_{\boldsymbol{u}}^n - \xi_{\boldsymbol{u}}^{n-1}), \theta_p^n\big),\\
\mathbb{T}_5 &= \sum_{n=1}^{m} \bigg(\int_{t^{n-1}}^{t^n} (t^{n-1}-s)\nabla\cdot(\partial_{tt}\boldsymbol{u})(s)ds, \theta_p^n \bigg).
\end{aligned}
$$

To bound the first term $\mathbb{T}_1$, we need the following equality:

$$
\sum_{n=1}^{m} (f^n - f^{n-1})g^{n-1} = f^m g^m - f^0 g^0 - \sum_{n=1}^{m} f^n (g^n - g^{n-1}). \tag{5.28}
$$

Moreover, recall the Taylor's expansion

$$
\frac{\xi_{\boldsymbol{u}}^n - \xi_{\boldsymbol{u}}^{n-1}}{\Delta t} = \partial_t \xi_{\boldsymbol{u}}^n + \frac{1}{\Delta t}\int_{t^{n-1}}^{t^n} (t^{n-1}-s)\partial_{tt}\xi_{\boldsymbol{u}}(s)ds \tag{5.29}
$$

with $\partial_t \xi_{\boldsymbol{u}}^n = \partial_t \xi_{\boldsymbol{u}}(t_n)$. Then, using (5.28), (5.29), (5.5) and Young's inequality, and noting that $\theta_{\boldsymbol{u}}^0 = 0$, we infer that

$$
\begin{aligned}
\mathbb{T}_1 &= -\sum_{n=1}^{m} a_h^{\boldsymbol{u}}\big(\xi_{\boldsymbol{u}}^n, \theta_{\boldsymbol{u}}^n - \theta_{\boldsymbol{u}}^{n-1}\big)\\
&= -a_h^{\boldsymbol{u}}\big(\xi_{\boldsymbol{u}}^m, \theta_{\boldsymbol{u}}^m\big) + \sum_{n=1}^{m} a_h^{\boldsymbol{u}}(\xi_{\boldsymbol{u}}^n - \xi_{\boldsymbol{u}}^{n-1}, \theta_{\boldsymbol{u}}^{n-1})\\
&\le \epsilon_1 \|\theta_{\boldsymbol{u}}^m\|_{\boldsymbol{V}}^2 + C\Bigg(\|\xi_{\boldsymbol{u}}^m\|_{\boldsymbol{V}}^2 + (\Delta t)^2 \int_0^{t^m} \|\partial_{tt}\xi_{\boldsymbol{u}}(s)\|_{\boldsymbol{V}}^2 ds\\
&\qquad\qquad + \Delta t \sum_{n=1}^{m} \|\partial_t \xi_{\mathbf{u}}^n\|_{\boldsymbol{V}}^2 + \Delta t \sum_{n=1}^{m-1} \|\theta_{\mathbf{u}}^n\|_{\boldsymbol{V}}^2 \Bigg).
\end{aligned} \tag{5.30}
$$

Similarly, since $\theta_{\boldsymbol{u}}^0 = 0$, then $\mathbb{T}_2$ can be bounded as follows:

$$
\begin{aligned}
\mathbb{T}_2 &= \sum_{n=1}^{m} \big(\xi_p^n, \nabla_h \cdot (\theta_{\boldsymbol{u}}^n - \theta_{\boldsymbol{u}}^{n-1})\big)\\
&= \big(\xi_p^m, \nabla_h \cdot \theta_{\boldsymbol{u}}^m\big) - \sum_{n=1}^{m} \big(\xi_p^n - \xi_p^{n-1}, \nabla_h \cdot \theta_{\boldsymbol{u}}^{n-1}\big)\\
&\le \epsilon_2 \|\theta_{\boldsymbol{u}}^m\|_{\boldsymbol{V}}^2 + C\Bigg(\|\xi_p^m\|_0^2 + (\Delta t)^2 \int_0^{t^m} \|\partial_{tt}\xi_p(s)\|_0^2 ds\\
&\qquad\qquad + \Delta t \sum_{n=1}^{m} \|\partial_t \xi_p^n\|_0^2 + \Delta t \sum_{n=1}^{m-1} \|\theta_{\mathbf{u}}^n\|_{\boldsymbol{V}}^2 \Bigg).
\end{aligned} \tag{5.31}
$$

Applying some techniques used in (5.14), utilizing (5.16), and Young's inequality, we deduce that

$$
\mathbb{T}_3 = \sum_{n=1}^{m} \sum_{K\in\mathcal{T}_h} \sum_{e\in\partial K\setminus\Gamma_t} \big\langle \boldsymbol{\sigma}^n \boldsymbol{n}_K, \theta_{\boldsymbol{u}}^n - \theta_{\boldsymbol{u}}^{n-1} \big\rangle_e
$$

$$
\begin{aligned}
&= \sum_{K\in\mathcal{T}_h}\sum_{e\in\partial K\setminus\Gamma_t} \left\langle \boldsymbol{\sigma}^m\boldsymbol{n}_K, \theta_{\boldsymbol{u}}^m\right\rangle_e - \sum_{n=1}^{m}\sum_{K\in\mathcal{T}_h}\sum_{F\in\partial K\setminus\Gamma_t} \left\langle (\boldsymbol{\sigma}^n-\boldsymbol{\sigma}^{n-1})\boldsymbol{n}_K, \theta_{\boldsymbol{u}}^{n-1}\right\rangle_e \\
&= \sum_{K\in\mathcal{T}_h}\sum_{e\in\partial K\setminus\Gamma_t} \left\langle (\boldsymbol{\sigma}^m-\overline{\boldsymbol{\sigma}^m})\boldsymbol{n}_K, \theta_{\boldsymbol{u}}^m-\overline{\theta_{\boldsymbol{u}}^m}\right\rangle_e \\
&\quad -\sum_{n=1}^{m}\sum_{K\in\mathcal{T}_h}\sum_{F\in\partial K\setminus\Gamma_t} \left\langle \left(\boldsymbol{\sigma}^n-\boldsymbol{\sigma}^{n-1}-\overline{\boldsymbol{\sigma}^n-\boldsymbol{\sigma}^{n-1}}\right)\boldsymbol{n}_K, \theta_{\boldsymbol{u}}^{n-1}-\overline{\theta_{\boldsymbol{u}}^{n-1}}\right\rangle_e \\
&\le \epsilon_3\|\theta_{\boldsymbol{u}}^m\|_{\boldsymbol{V}}^2 + C\Bigg(h^2\big(2\mu|\boldsymbol{u}^m|_2^2+\lambda|\nabla\cdot\boldsymbol{u}^m|_1^2\big) \\
&\qquad + h^2\int_0^{t^m}\big(2\mu|\partial_t\boldsymbol{u}(s)|_2^2+\lambda|\nabla\cdot(\partial_t\boldsymbol{u})(s)|_1^2\big)ds + \Delta t\sum_{n=0}^{m-1}\|\theta_{\boldsymbol{u}}^n\|_{\boldsymbol{V}}^2\Bigg). \qquad (5.32)
\end{aligned}
$$

Application of (5.29) for $\mathbb{T}_4$ yields

$$
\begin{aligned}
\mathbb{T}_4 &= -\sum_{n=1}^{m}\big(\nabla_h\cdot(\xi_{\boldsymbol{u}}^n-\xi_{\boldsymbol{u}}^{n-1}),\theta_p^n\big) \\
&\le C\Bigg((\Delta t)^2\int_0^{t^m}\|\partial_{tt}\xi_{\boldsymbol{u}}(s)\|_{\boldsymbol{V}}^2ds + \Delta t\sum_{n=1}^{m}\big(\|\theta_p^n\|_0^2+\|\partial_t\xi_{\boldsymbol{u}}^n\|_{\boldsymbol{V}}^2\big)\Bigg). \qquad (5.33)
\end{aligned}
$$

It follows from the Cauchy-Schwarz inequality that

$$
\begin{aligned}
\mathbb{T}_5 &= \sum_{n=1}^{m}\left(\int_{t^{n-1}}^{t^n}(t^{n-1}-s)\nabla\cdot(\partial_{tt}\boldsymbol{u})(s)ds,\theta_p^n\right) \\
&\le \sum_{n=1}^{m}\left\|\int_{t^{n-1}}^{t^n}(t^{n-1}-s)\nabla\cdot(\partial_{tt}\boldsymbol{u})(s)ds\right\|_0\|\theta_p^n\|_0.
\end{aligned}
$$

Moreover, there holds

$$
\left\|\int_{t^{n-1}}^{t^n}(t^{n-1}-s)\nabla\cdot(\partial_{tt}\boldsymbol{u})(s)ds\right\|_0 \le (\Delta t)^{\frac{3}{2}}\left(\int_{t^{n-1}}^{t^n}\|\nabla\cdot(\partial_{tt}\boldsymbol{u})(s)\|_0^2ds\right)^{\frac{1}{2}}.
$$

Thus, we further deduce that

$$
\mathbb{T}_5 \le C\Bigg(\Delta t\sum_{n=1}^{m}\|\theta_p^n\|_0^2 + (\Delta t)^2\int_0^{t^m}\|\nabla\cdot(\partial_{tt}\boldsymbol{u})(s)\|_0^2ds\Bigg). \qquad (5.34)
$$

On the other hand, subtracting (4.1) from (5.5) leads to

$$
a_h^{\boldsymbol{u}}(\theta_{\boldsymbol{u}}^n,\boldsymbol{v}_h) = -b_h(\boldsymbol{v}_h,\theta_p^n). \qquad (5.35)
$$

By using the inf-sup condition (4.6), we see that

$$
\|\theta_p^n\|_0 \le \frac{1}{\alpha_0}\sup_{\boldsymbol{v}_h\in\boldsymbol{V}_h}\frac{b_h(\boldsymbol{v}_h,\theta_p^n)}{\|\boldsymbol{v}_h\|_{\boldsymbol{V}}} = \frac{1}{\alpha_0}\sup_{\boldsymbol{v}_h\in\boldsymbol{V}_h}\frac{-a_h^{\boldsymbol{u}}(\theta_{\boldsymbol{u}}^n,\boldsymbol{v}_h)}{\|\boldsymbol{v}_h\|_{\boldsymbol{V}}} = \frac{1}{\alpha_0}\|\theta_{\boldsymbol{u}}^n\|_{\boldsymbol{V}}. \qquad (5.36)
$$

Combining (5.27), (5.30)-(5.34), and (5.36), we have

$$
(1-\epsilon_1-\epsilon_2-\epsilon_3)\|\theta_{\boldsymbol{u}}^m\|_{\boldsymbol{V}}^2 + \Delta t\sum_{n=1}^{m}\|\theta_p^n\|_Q^2
$$

$$\leq C\bigg(\Delta t\sum_{n=1}^{m}\|\theta_{\boldsymbol{u}}^n\|_{\boldsymbol{V}}^2+\|\xi_{\boldsymbol{u}}^m\|_{\boldsymbol{V}}^2+\|\xi_p^m\|_Q^2+\Delta t\sum_{n=1}^{m}\big(\|\partial_t\xi_{\mathbf{u}}^n\|_{\boldsymbol{V}}^2+\|\partial_t\xi_p^n\|_0^2\big)$$
$$+(\Delta t)^2\int_0^{t^m}\|\partial_{tt}\xi_p(s)\|_0^2ds+(\Delta t)^2\int_0^{t^m}\|\nabla\cdot(\partial_{tt}\boldsymbol{u})(s)\|_0^2ds$$
$$+(\Delta t)^2\int_0^{t_m}\|\partial_{tt}\xi_{\boldsymbol{u}}(s)\|_{\boldsymbol{V}}^2ds+h^2\big(2\mu|\boldsymbol{u}^m|_2^2+\lambda|\nabla\cdot\boldsymbol{u}^m|_1^2\big)$$
$$+h^2\int_0^{t^m}\big(2\mu|\partial_t\boldsymbol{u}(s)|_2^2+\lambda|\nabla\cdot\partial_t\boldsymbol{u}(s)|_1^2\big)ds\bigg). \tag{5.37}$$

Choosing ϵ_i, $i=1,2,3$ such that $1-\epsilon_1-\epsilon_2-\epsilon_3>0$, then using the discrete Gronwall's inequality [23, 28], some approximation properties (see (5.8)-(5.10)), and noting that (5.37) holds for any $1\leq m\leq N$, we conclude that

$$\max_{1\leq n\leq N}\|\theta_{\boldsymbol{u}}^n\|_{\boldsymbol{V}}^2+\Delta t\sum_{n=1}^{N}\|\theta_p^n\|_Q^2\leq C\big(h^2\Phi_1+(\Delta t)^2\Phi_2\big), \tag{5.38}$$

where

$$\Phi_1=\max_{1\leq m\leq N}\big(2\mu\|\boldsymbol{u}^m\|_2^2+\lambda\|\nabla\cdot\boldsymbol{u}^m\|_1^2\big)$$
$$+\bigg(\int_0^T\big(2\mu|\partial_t\boldsymbol{u}(s)|_2^2+\lambda|\nabla\cdot(\partial_t\boldsymbol{u})(s)|_1^2\big)ds\bigg)+\max_{1\leq m\leq N}\|p^m\|_2^2, \tag{5.39}$$
$$\Phi_2=h^4\int_0^T\|\partial_{tt}p(s)\|_2^2ds+\int_0^T\|\nabla\cdot(\partial_{tt}\boldsymbol{u})(s)\|_0^2ds$$
$$+h^2\int_0^T 2\mu|\partial_{tt}\boldsymbol{u}(s)|_2^2+\lambda|\nabla\cdot(\partial_{tt}\boldsymbol{u})(s)|_1^2ds. \tag{5.40}$$

Combining this bound with the error estimates for $\xi_p^n,\xi_{\boldsymbol{u}}^n$ (see Lemma 5.1), and using the triangle inequality, we obtain

$$\max_{1\leq n\leq N}\|\boldsymbol{u}^n-\boldsymbol{u}_h^n\|_{\boldsymbol{V}}^2+\Delta t\sum_{n=1}^{N}\|p^n-p_h^n\|_Q^2\leq C_{\mathrm{a}}\big(h^2\Phi_1+(\Delta t)^2\Phi_2\big), \tag{5.41}$$

which is the desired estimate (5.18). □

5.2. Error estimates for $c_0>0$

When $c_0>0$, proceeded as in Theorem 5.3, we have a result analogous to (5.27)

$$\frac{1}{2}a_h^{\boldsymbol{u}}(\theta_{\boldsymbol{u}}^m,\theta_{\boldsymbol{u}}^m)+\frac{c_0}{2}\|\theta_p^m\|_0^2+\Delta t\sum_{n=1}^{m}\|\theta_p^n\|_Q^2\leq\mathbb{T}_1+\mathbb{T}_2+\mathbb{T}_3+\mathbb{T}_4+\mathbb{T}_5. \tag{5.42}$$

Based on this formulation, utilizing a similar derivation procedure as that in Theorem 5.3, we obtain a slightly stronger conclusion for this case.

Theorem 5.4. *Let $(\boldsymbol{u},p)\in\boldsymbol{V}\times Q$ and $(\boldsymbol{u}_h^n,p_h^n)\in\boldsymbol{V}_h\times Q_h$ be the solutions of* (2.1)-(2.2) *and* (3.1)-(3.2)*, respectively. Under the assumptions stated in Theorem* 5.3*, it holds that*

$$\max_{1\leq n\leq N}\|\boldsymbol{u}^n-\boldsymbol{u}_h^n\|_{\boldsymbol{V}}^2+\max_{1\leq n\leq N}\|p^n-p_h^n\|_0^2+\Delta t\sum_{n=1}^{N}\|p^n-p_h^n\|_Q^2\leq C_{\mathrm{b}}\big(h^2\Phi_1+(\Delta t)^2\Phi_3\big). \tag{5.43}$$

Here,

$$\Phi_3 = \Phi_2 + \int_0^T \|\partial_{tt} p(s)\|_0^2 ds$$

with Φ_2 *being defined in* (5.40).

Now, we show that the functions Φ_1, Φ_2 (see (5.18)) and Φ_3 (see (5.43)) can be bounded by the constants independent of λ. For Φ_1, it satisfies

$$\begin{aligned}\Phi_1 = & \max_{1\le m\le N} \left(2\mu\|\boldsymbol{u}^m\|_2^2 + \lambda\|\nabla\cdot\boldsymbol{u}^m\|_1^2\right) \\ & + \left(\int_0^T (2\mu|\partial_t \boldsymbol{u}(s)|_2^2 + \lambda|\nabla\cdot(\partial_t\boldsymbol{u})(s)|_1^2)ds\right) + \max_{1\le m\le N}\|p^m\|_2^2 \\ \triangleq & \ \Phi_{11} + \Phi_{12} + \Phi_{13}.\end{aligned} \tag{5.44}$$

The λ independent bounds for Φ_{11}, Φ_{12} and Φ_{13} can be derived from Theorem 5.1, Remarks 5.1 and 5.2, respectively. For Φ_2, we have

$$\begin{aligned}\Phi_2 = & \ h^4\int_0^T \|\partial_{tt}p(s)\|_2^2 ds + \int_0^T \|\nabla\cdot(\partial_{tt}\boldsymbol{u})(s)\|_0^2 ds \\ & + h^2\int_0^T 2\mu|\partial_{tt}\boldsymbol{u}(s)|_2^2 + \lambda|\nabla\cdot(\partial_{tt}\boldsymbol{u})(s)|_1^2 ds \\ \triangleq & \ \Phi_{21} + \Phi_{22} + \Phi_{23}.\end{aligned} \tag{5.45}$$

The λ independent bound for Φ_{21} is obtained from Remark 5.2, and the bounds for Φ_{22} and Φ_{23} are derived from Remark 5.1. Since

$$\Phi_3 = \Phi_2 + \int_0^T \|\partial_{tt} p(s)\|_0^2 ds,$$

the bounds for $\int_0^T \|\partial_{tt}p(s)\|_0^2 ds$ (see Remark 5.2) and Φ_2 gives the desired estimate for Φ_3.

Remark 5.3. Here, we also needed to use Gronwall's inequality [23, 28] in (5.37) to derive the error estimates. The constants C_{a} (in (5.18)) and C_{b} (in (5.43)) depend on the exponentially growing factor $\exp(\sum_{n=1}^N(\Delta t/(1-\Delta t)))$, which is independent of λ. Furthermore, we used the regularity results in [55] to prove that the functions Φ_1, Φ_2 and Φ_3 are bounded by the constants independent of λ. Thus, our estimates stated in Theorems 5.3 and 5.4 depend on the parameter μ, but are robust in the limit that $\lambda \to \infty$.

Remark 5.4. In this paper, we combine the CR and the conforming $\mathbb{P}_1$ finite elements to discretize the Biot model. This method is not a mass-conserved scheme, which is a disadvantage of the proposed method. However, it is worth mentioning that, if the displacement approximation is replaced by interior penalty DG (IPDG) method (with linear discontinuous finite element), the error analysis in this work can be extended to such a case with minor modifications. In fact, the IPDG-$\mathbb{P}_1$ pair also satisfies inf-sup condition (see [16]), and IPDG can also overcome Possion locking in linear elasticity. Thus, our work can be seen as an extension of the two-field MINI elements [48] to the CR-$\mathbb{P}_1$ and IPDG-$\mathbb{P}_1$ schemes. Comparing with the three-field CR-RT-$\mathbb{P}_0$ scheme [48], we can approximate the pressure with second-order accuracy in the L^2 sense (see the numerical results), while the CR-RT-$\mathbb{P}_0$ scheme only has a first-order accuracy.

Remark 5.5. In the following numerical tests, we observed that the pressure has the second-order accuracy in L^2 norm, see Tables 6.1-6.3. We may resort to recent work [53] to prove this result in a rigorous theory. This issue is an interesting topic which involve some Aubin-Nitsche arguments, but another long story. We will carefully investigate the theoretical analysis in a future work.

6. Numerical Experiments

To test the accuracy of our method, we introduce the following benchmark model. The true solution is the same as that in [54], although the coefficient setting and the boundary condition are slightly different (but will not affect the conclusions on accuracy). In the following, we use $Q_{\mathbf{r}} = \lambda/\mu$ to denote the quotient of the Lamé constants.

Example 6.1. Let $\Omega = (0,1) \times (0,1)$ with the boundary being

$$\Gamma_1 = \{(1,y); 0 \le y \le 1\}, \quad \Gamma_2 = \{(x,0); 0 \le x \le 1\},$$
$$\Gamma_3 = \{(0,y); 0 \le y \le 1\}, \quad \Gamma_4 = \{(x,1); 0 \le x \le 1\}.$$

The force term $\boldsymbol{f}$ and g in (2.1)-(2.2) are chosen such that the exact solution is given by

$$\boldsymbol{u} = e^{-t} \begin{pmatrix} c\sin(2\pi y)\big(\cos(2\pi x) - 1\big) + \dfrac{1}{\mu+\lambda}\sin(\pi x)\sin(\pi y) \\ \sin(2\pi x)\big(1 - \cos(2\pi y)\big) + \dfrac{1}{\mu+\lambda}\sin(\pi x)\sin(\pi y) \end{pmatrix},$$
$$p = e^{-t}\sin(\pi x)\sin(\pi y).$$

Note that the solution is designed to satisfy $\mathrm{div}\boldsymbol{u} = \pi e^{-t}\sin(\pi(x+y))/(\mu+\lambda) \to 0$ as $\lambda \to +\infty$ at any time t. Pure Dirichlet boundary condition is imposed. As the key parameters are the Poisson ratio ν and the permeability $\boldsymbol{K}$, the parameters E is fixed to be 1. In all the tests, uniform grids with an initial size $h = 1/8$ are used. The mesh refinement is based on linking the midpoints of the edges.

In Tables 6.1 and 6.2, we test the approximation properties of our method under different Poisson ratios. The hydraulic conductivity is fixed to be $\boldsymbol{K} = \boldsymbol{I}$ and the time step is fixed to be $\Delta t = 1.0 \times 10^{-4}$. We test both the compressible case ($\nu = 0.3$) and the almost incompressible case ($\nu = 0.499$). The test results are obtained by using (3.1)-(3.2). Tables 6.1 and 6.2 correspond to the numerical errors and the convergence orders for the case $\nu = 0.3$ and $\nu = 0.499$ separately. From the numerical results, we observe that no matter $\nu = 0.499$ or $\nu = 0.3$, the H^1 error orders of $\boldsymbol{u}$ and p are around 1, while the L^2 error orders of $\boldsymbol{u}$ and p are around 2. This means that the numerical results exhibit optimal approximation orders in both the energy norm and the L^2 norm.

In Table 6.3, we test the approximation properties of our method under a small permeability, which usually causes pressure oscillations. The hydraulic conductivity is set be $\boldsymbol{K} = 10^{-6}\boldsymbol{I}$ and the time step is again $\Delta t = 1.0 \times 10^{-4}$. The Poisson ratio is set to be $\nu = 0.3$. The numerical errors and the convergence orders are reported in Table 6.3. The test results are obtained by using (3.6)-(3.7). From the numerical results, we observe that the H^1 and L^2 error orders of $\boldsymbol{u}$ are optimal. The H^1 error orders of p are around 1, while the L^2 error orders of p are smaller than 2. This means that the numerical results exhibit optimal approximation orders in the energy norm.

Table 6.1: Rate of convergence for $\nu = 0.3$ ($Q_{\mathbf{r}} = 5$) , fixed $\boldsymbol{K} = \boldsymbol{I}$.

N	L^2 & H^1 errs of $\boldsymbol{u}$	Orders	L^2 & H^1 errs of p	Orders
8	5.329e-2 & 2.223e+0		5.039e-2 & 7.099e-1	
16	1.360e-2 & 1.108e+0	1.97 & 1.00	1.361e-2 & 2.802e-1	1.89 & 1.34
32	3.432e-3 & 5.526e-1	1.99 & 1.00	3.540e-3 & 1.200e-1	1.94 & 1.22
64	8.613e-4 & 2.759e-1	1.99 & 1.00	8.950e-4 & 5.588e-2	1.98 & 1.10
128	2.157e-4 & 1.378e-1	2.00 & 1.00	2.244e-4 & 2.736e-2	2.00 & 1.03

Table 6.2: Rate of convergence for $\nu = 0.499$ ($Q_{\mathbf{r}} = 999.999$), fixed $\boldsymbol{K} = \boldsymbol{I}$.

N	L^2 & H^1 errs of $\boldsymbol{u}$	Orders	L^2 & H^1 errs of p	Orders
8	5.599e-2 & 2.204e+0		2.095e-2 & 4.306e-1	
16	1.445e-2 & 1.101e+0	1.95 & 1.00	5.329e-3 & 2.167e-1	1.98 & 0.99
32	3.659e-3 & 5.491e-1	1.98 & 1.00	1.338e-3 & 1.086e-1	1.99 & 1.00
64	9.191e-4 & 2.741e-1	1.99 & 1.00	3.349e-4 & 5.430e-2	2.00 & 1.00
128	2.302e-4 & 1.369e-1	2.00 & 1.00	8.374e-5 & 2.715e-2	2.00 & 1.00

Table 6.3: Rate of convergence for $\boldsymbol{K} = 10^{-6}\boldsymbol{I}$, fixed $\nu = 0.3$ ($Q_{\mathbf{r}} = 5$).

N	L^2 & H^1 errs of $\boldsymbol{u}$	Orders	L^2 & H^1 errs of p	Orders
8	5.252e-2 & 2.214e+0		2.342e-2 & 4.927e-1	
16	1.339e-2 & 1.104e+0	1.97 & 1.00	9.922e-3 & 2.564e-1	1.24 & 0.94
32	3.385e-3 & 5.509e-1	1.98 & 1.00	3.318e-3 & 1.287e-1	1.58 & 0.99
64	8.514e-4 & 2.751e-1	1.99 & 1.00	9.854e-4 & 6.485e-2	1.75 & 0.99
128	2.135e-4 & 1.374e-1	2.00 & 1.00	2.819e-4 & 3.367e-2	1.81 & 0.95

To further check whether the proposed method can resolve the pressure oscillation problem in solving the Biot model, we consider the cantilever bracket problem [19, 55]. In our tests, all settings including physical parameters, boundary and initial conditions, and discretization parameters, are the same as those in [19, 55].

Example 6.2. The computational domain and Γ are the same as those in Example 6.1. The material parameters are

$$E = 10^5, \quad \nu = 0.4, \quad c_0 = 0, \quad \alpha = 1.0, \quad \boldsymbol{K} = 1 \times 10^{-7}\boldsymbol{I}, \quad \Delta t = 0.001.$$

Thus, the quotient of the Lamé constants $Q_{\mathbf{r}} = \lambda/\mu = 10$. There is no force term or source term, that is, $\boldsymbol{f} = \mathbf{0}$ and $g = 0$. The boundary conditions are taken as

$$\begin{aligned}
&\nabla p \cdot \boldsymbol{n} = 0 && \text{on } \partial\Omega, \\
&\boldsymbol{u} = \mathbf{0} && \text{on } \Gamma_3 \times (0, T), \\
&\sigma\boldsymbol{n} - \alpha p\boldsymbol{n} = \boldsymbol{h} && \text{on } \Gamma_j \times (0, T), \quad j = 1, 2, 4,
\end{aligned}$$

where $\boldsymbol{h} = (h_1, h_2)$ with

$$h_1 = 0 \qquad \text{on } \Gamma_j, \qquad\qquad j = 1, 2, 4,$$
$$h_2 = \begin{cases} 0 & \text{on } \Gamma_j \times (0, T), \quad j = 1, 2, \\ -1 & \text{on } \Gamma_4 \times (0, T). \end{cases}$$

The zero initial conditions are assigned for both $\boldsymbol{u}$ and p [19, 55].

In the numerical simulation, we set $h = 1/32$, $\Delta t = 0.001$, and run 1 step of time evolution. The test results are obtained by using (3.6)-(3.7). In Fig. 6.1, we display the surface and color plot of the computed pressure by using the proposed stabilized finite element method. From the results, one can see clearly that the numerical solutions do not suffer from pressure oscillation.

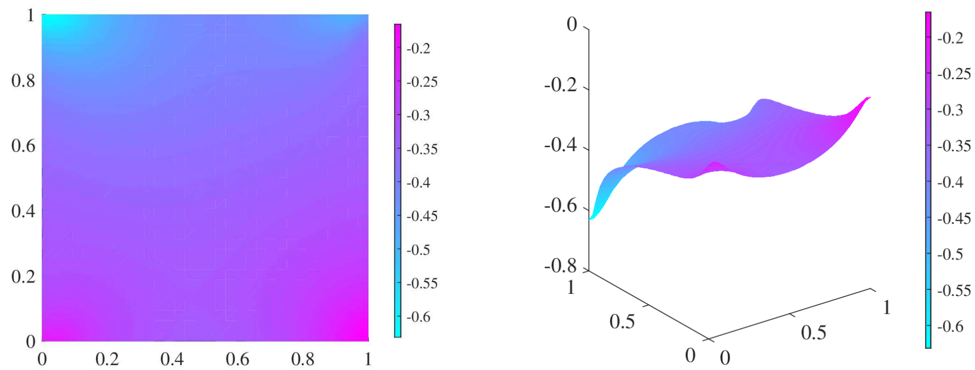

(a) The color plot of pressure. (b) The surface plot of pressure.

Fig. 6.1. The pressure distribution for Example 6.2.

7. Concluding Remarks

In this work, we propose and analyze a mixed finite element method for solving the Biot consolidation model. In our method, the solid displacement is discretized by the nonconforming CR element, while the fluid pressure is approximated by a linear conforming element. The existence and uniqueness of solutions of the fully discrete scheme are established. Then, under some assumptions on the regularities of the solutions, we derive optimal order a priori error estimates for each variable. In future work, we will concentrate on developing the corresponding a posteriori error estimates.

Acknowledgements. The work of Y. Zeng is supported by the Guangdong Basic and Applied Basic Research Foundation (Grant No. 2020A1515011032). The work of M. Cai is supported in part by the NIH-BUILD Grant through UL1GM118973, by the NIH-RCMI Grant through U54MD013376, and by the National Science Foundation awards (Grant Nos. 1700328, 1831950). The work of L. Zhong is supported by the National Natural Science Foundation of China (Grant No. 12071160).

References

[1] J.H. Adler, F.J. Gaspar, X. Hu, P. Ohm, C. Rodrigo, and L.T. Zikatanov, Robust preconditioners for a new stabilized discretization of the poroelastic equations, *SIAM J. Sci. Comput.*, **42** (2020), B761–B791.

[2] G. Aguilar, F. Gaspar, F. Lisbona, and C. Rodrigo, Numerical stabilization of Biots consolidation model by a perturbation on the flow equation, *Internat. J. Numer. Methods Engrg.*, **75** (2008), 1282–1300.

[3] T. Bærland, J.J. Lee, K.A. Mardal, and R. Winther, Weakly imposed symmetry and robust preconditioners for Biot's consolidation model, *Comput. Methods Appl. Math.*, **17** (2017), 377–396.

[4] M.A. Biot, Theory of elasticity and consolidation for a porous anisotropic solid, *J. Appl. Phys.*, **26** (1955), 182–185.

[5] D. Boffi, M. Botti, and D.A. Di Pietro, A nonconforming high-order method for the Biot problem on general meshes, *SIAM J. Sci. Comput.*, **38** (2016), A1508–A1537.

[6] S.C. Brenner, Korn's inequalities for piecewise H^1 vector fields, *Math. Comp.*, **73** (2003), 1067–1087.

[7] S.C. Brenner, Forty years of the Crouzeix-Raviart element, *Numer. Methods Partial Differential Equations*, **31** (2015), 367–396.

[8] S.C. Brenner and L.R. Scott, *The Mathematical Theory of Finite Element Methods*, Springer-Verlag, 2008.

[9] S.C. Brenner and L.Y. Sung, Linear finite element methods for planar linear elasticity, *Math. Comp.*, **59** (1992), 321–338.

[10] R. Bürger, S. Kumar, D. Mora, and N. Verma, Virtual element methods for the three-field formulation of time-dependent linear poroelasticity, *Adv. Comput. Math.*, **47** (2021), 2.

[11] N. Chaabane and B. Rivière, A sequential discontinuous Galerkin method for the coupling of flow and geomechanics, *J. Sci. Comput.*, **74** (2018), 375–395.

[12] S. Chen, Q. Hong, J. Xu, and K. Yang, Robust block preconditioners for poroelasticity, *Comput. Methods Appl. Mech. Engrg.*, **369** (2020), 113229.

[13] Y. Chen, G. Chen, and X. Xie, Weak Galerkin finite element method for Biot's consolidation problem, *J. Comput. Appl. Math.*, **330** (2018), 398–416.

[14] Y. Chen, Y. Luo, and M. Feng, Analysis of a discontinuous Galerkin method for the Biot's consolidation problem, *Appl. Math. Comput.*, **219** (2013), 9043–9056.

[15] M. Crouzeix and P.-A. Raviart, Conforming and nonconforming finite elements methods for solving the stationary Stokes equation I, *RAIRO Numér. Anal.*, **7** (1973), 33–75.

[16] D.A. Di Pietro and A. Ern, *Mathematical Aspects of Discontinuous Galerkin Methods*, Springer-Verlag, 2012.

[17] L.C. Evans, *Partial Differential Equations*, in: *Graduate Studies in Mathematics*, Vol. 19, AMS, 2010.

[18] R.S. Falk, Nonconforming finite element methods for the equations of linear elasticity, *Math. Comp.*, **57** (1991), 529–550.

[19] X. Feng, Z. Ge, and Y. Li, Analysis of a multiphysics finite element method for a poroelasticity model, *IMA J. Numer. Anal.*, **38** (2018), 330–359.

[20] Y. Guo and J. Huang, A robust finite element method for elastic vibration problems, *Comput. Methods Appl. Math.*, **20** (2020), 481–500.

[21] J. Haga, H. Osnes, and H. Langtangen, On the causes of pressure oscillations in low-permeable and low-compressible porous media, *Int. J. Numer. Anal. Methods Geomech.*, **36** (2012), 1507–1522.

[22] P. Hansbo and M.G. Larson, Discontinuous Galerkin and the Crouzeix-Raviart element: Application to elasticity, *ESAIM Math. Model. Numer. Anal.*, **37** (2003), 63–72.

[23] J.G. Heywood and R. Rannacher, Finite-element approximation of the nonstationary Navier-Stokes problem. Part IV: Error analysis for second-order time discretization, *SIAM J. Numer. Anal.*, **27** (1990), 353–384.

[24] Q. Hong and J. Kraus, Parameter-robust stability of classical three-field formulation of Biot's consolidation model, *Electron. Trans. Numer. Anal.*, **48** (2018), 202–226.

[25] Q. Hong, J. Kraus, M. Lymbery, and F. Philo, Parameter-robust Uzawa-type iterative methods for double saddle point problems arising in Biot's consolidation and multiple-network poroelasticity models, *Math. Models Methods Appl. Sci.*, **30** (2020), 2523–2555.

[26] X. Hu, L. Mu, and X. Ye, Weak Galerkin method for the Biot's consolidation model, *Comput. Math. Appl.*, **75** (2018), 2017–2030.

[27] X. Hu, C. Rodrigo, F.J. Gaspar, and L.T. Zikatanov, A nonconforming finite element method for the Biot's consolidation model in poroelasticity, *J. Comput. Appl. Math.*, **310** (2017), 143–154.

[28] V. John, *Finite Element Methods for Incompressible Flow Problems*, Springer-Verlag, 2016.

[29] G. Ju, M. Cai, J. Li, and J. Tian, Parameter-robust multiphysics algorithms for Biot model with application in brain edema simulation, *Math. Comput. Simul.*, **177** (2020), 385–403.

[30] G. Kanschat and B. Rivière, A finite element method with strong mass conservation for Biot's linear consolidation model, *J. Sci. Comput.*, **77** (2018), 1762–1779.

[31] J. Korsawe and G. Starke, A least-squares mixed finite element method for Biot's consolidation problem in porous media, *SIAM J. Numer. Anal.*, **43** (2005), 318–339.

[32] J. Korsawe, G. Starke, W. Wang, and O. Kolditz, Finite element analysis of poro-elastic consolidation in porous media: Standard and mixed approaches, *Comput. Methods Appl. Mech. Engrg.*, **195** (2006), 1096–1115.

[33] S. Kumar, R. Oyarzúa, R. Ruiz-Baier, and R. Sandilya, Conservative discontinuous finite volume and mixed schemes for a new four-field formulation in poroelasticity, *ESAIM Math. Model. Numer. Anal.*, **54** (2020), 273–299.

[34] B.P. Lamichhane, A nonconforming finite element method for the Stokes equations using the Crouzeix-Raviart element for the velocity and the standard linear element for the pressure, *Int. J. Numer. Methods Fluids*, **74** (2014), 222–228.

[35] J.J. Lee, Robust error analysis of coupled mixed methods for Biot's consolidation model, *J. Sci. Comput.*, **69** (2016), 610–632.

[36] J.J. Lee, Robust three-field finite element methods for Biot's consolidation model in poroelasticity, *BIT Numer. Math.*, **58** (2018), 347–372.

[37] J.J. Lee, K.A. Mardal, and R. Winther, Parameter-robust discretization and preconditioning of Biot's consolidation model, *SIAM J. Sci. Comput.*, **39** (2017), A1–A24.

[38] J. Li and Z. Chen, A new local stabilized nonconforming finite element method for the Stokes equations, *Computing*, **82** (2008), 157–170.

[39] K.A. Mardal and R. Winther, An observation on Korn's inequality for nonconforming finite element methods, *Math. Comp.*, **75** (2006), 1–6.

[40] M.A. Murad and A.F.D. Loula, Improved accuracy in finite element analysis of Biot's consolidation problem, *Comput. Methods Appl. Mech. Engrg.*, **95** (1992), 359–382.

[41] M.A. Murad and A.F.D. Loula, On stability and convergence of finite element approximations of Biot's consolidation problem, *Internat. J. Numer. Methods Engrg.*, **37** (1994), 645–667.

[42] M.A. Murad, V. Thomée, and A.F.D. Loula, Asymptotic behavior of semidiscrete finite-element approximations of Biot's consolidation problem, *SIAM J. Numer. Anal.*, **33** (1996), 1065–1083.

[43] P.J. Phillips and M.F. Wheeler, A coupling of mixed and continuous Galerkin finite element methods for poroelasticity I: The continuous in time case, *Comput. Geosci.*, **11** (2007), 131–144.

[44] P.J. Phillips and M. F. Wheeler, A coupling of mixed and continuous Galerkin finite element methods for poroelasticity II: The discrete in time case, *Comput. Geosci.*, **11** (2007), 145–158.

[45] P.J. Phillips and M.F. Wheeler, A coupling of mixed and discontinuous Galerkin finite element methods for poroelasticity, *Comput. Geosci.*, **12** (2008), 417–435.

[46] P.J. Phillips and M.F. Wheeler, Overcoming the problem of locking in linear elasticity and poroelasticity: An heuristic approach, *Comput. Geosci.*, **13** (2009), 5–12.

[47] H. Qi, L. Wang, and W. Zheng, On locking-free fnite element schemes for three-dimensional elasticity, *J. Comput. Math.*, **23** (2005), 101–112.

[48] C. Rodrigo, F. Gaspar, X. Hu, L. Zikatanov, Stability and monotonicity for some discretizations of the Biot's consolidation model, *Comput. Methods Appl. Mech. Engrg.*, **298** (2016), 183–204.

[49] R.E. Showalter, Diffusion in poro-elastic media, *J. Math. Anal. Appl.*, **251** (2000), 310–340.

[50] M. Sun and H. Rui, A coupling of weak Galerkin and mixed finite element methods for poroelasticity, *Comput. Math. Appl.*, **73** (2017), 804–823.

[51] X. Tang, Z. Liu, B. Zhang, and M. Feng, On the locking-free three-field virtual element methods for Biot's consolidation model in poroelasticity, *ESAIM Math. Model. Numer. Anal.*, **55** (2021), 909–939.

[52] R. Wang, X. Wang, and R. Zhang, A modified weak Galerkin finite element method for the poroelasticity problems, *Numer. Math. Theory Methods Appl.*, **11** (2018), 518–539.

[53] M.F. Wheeler, V. Girault, and X. Lu, Optimal L^2 a priori error estimates for the Biot system, *La Matematica*, **1** (2022), 317–341.

[54] S.Y. Yi, A coupling of nonconforming and mixed finite element methods for Biot's consolidation model, *Numer. Methods Partial Differential Equations*, **29** (2013), 1749–1777.

[55] S.Y. Yi, A study of two modes of locking in poroelasticity, *SIAM J. Numer. Anal.*, **55** (2017), 1915–1936.

[56] Y. Zeng, M. Cai, and F. Wang, An H(div)-conforming finite element method for the Biot consolidation model, *East Asian J. Appl. Math.*, **9** (2019), 558–579.